X-ray-absorption spectroscopy and n-body distribution functions in condensed matter. II. Data analysis and applications

Adriano Filipponi*
Dipartimento di Fisica, Università degli Studi dell'Aquila, Via Vetoio, 67010 Coppito, L'Aquila, Italy

Andrea Di Cicco
Dipartimento di Matematica e Fisica, Università degli Studi di Camerino, Via Madonna delle Carceri, 62032 Camerino (MC), Italy
(Received 7 July 1994; revised manuscript received 11 August 1995)

The practical and theoretical aspects of the GNXAS method for multiple-scattering extended x-ray-absorption fine-structure (EXAFS) data analysis are treated in a comprehensive account. The model function used to fit the raw absorption coefficient is described and details on the least-squares fitting procedure and parameter definition are reported. Large emphasis is given, in EXAFS analysis, to the description of criteria for a complete statistical evaluation of the results, including error estimate and model evaluation. An extensive set of applications to prototypical molecular (Br_2, CS_2), and crystalline [c-Ge and Pd (fcc)] systems is reported. Structural parameters always coincide with the known values within statistical accuracy indicating that systematic errors due to approximations in the theory are negligible. The present results also demonstrate that x-ray absorption spectroscopy can provide information on three-body atomic arrangements like average geometrical and vibrational parameters with statistical significance. In all examples, despite the inclusion of several three-body contributions, the total number of fitting parameters does not exceed the information content of the spectra; details on error evaluation and correlation plots in the parameter space are reported.

I. INTRODUCTION

X-ray-absorption spectroscopy (XAS) has become a very popular technique, in combination with the data analysis of the extended x-ray-absorption fine-structure (EXAFS), to probe short-range structural properties around selected atomic species in condensed matter.[1] Typical applications span over several scientific subjects in physics, chemistry, and biology, including both fundamental and applied research. In recent times the necessity to establish standard procedures and criteria for EXAFS data analysis[2] has been pointed out.

Many recent efforts have been devoted to provide a solid theoretical foundation for the data-analysis procedures, with the ultimate scope of being able to perform an EXAFS data analysis based on theoretical signals rather than experimental models. This required advances in various fields, including the improvements in the modeling of the effective potential,[3,4] the inclusion of multiple-scattering (MS) pathways in the calculation of the signal,[5–8] and the developments of novel and more efficient algorithms.[9,10] One by-product of these theoretical efforts has been the implementation of data-analysis packages that include MS contributions. The three main packages developed so far present strong similarities, but also peculiar differences; they are, listed in temporal order, EXCURVE developed by the Daresbury group,[11] GNXAS (Refs. 12–14) developed by our group, and the EXAFS analysis package developed by the Seattle group[15,16] based on the FEFF codes.[17]

The GNXAS package has been applied, so far, to a large number of systems including simple molecules,[18–20] crystalline solids,[21,22] amorphous solids,[23] simple liquids,[24–27] molecular liquids,[28] aqueous solutions,[29,30] nanocrystalline systems,[31] and complex molecules or biological matter.[32,33] The success of the method is mainly due to the possibility of calculating the actual $\gamma^{(n)}$ signals associated with n-body configurations, that account for an infinite number of MS paths, and to the correct treatment of the configurational average of MS signals that allows us to fit correlated vibrational motion in three-body configurations.

The theoretical foundations of the GNXAS approach have been described in a previous paper,[14] hereafter referred to as I, including a full discussion of the most efficient algorithms to calculate the $\gamma^{(n)}$ signals and the procedures to perform configurational averages. In the present paper a complete description of the least-square fitting procedures will be reported. A particular emphasis is given to the criteria for the estimate of the errors on the optimal parameters based on the application of statistical tests. Finally a complete set of examples of data analysis performed on prototypical molecules or crystalline structures is presented. This paper in combination with I is intended to provide a full reference for future applications of the GNXAS method.

The reported experimental spectra are mostly unpublished results, collected by the authors at international synchrotron radiation facilities in the past few years. In particular measurements have been performed at the LURE (Orsay, France) beamlines D42-EXAFS 1 equipped with a Si (331) monochromator and D44-EXAFS 4 equipped with a Si (311) monochromator and at the PULS (Progetto Utilizzazione Luce di Sincrotrone) x-ray beamline equipped with a Si (111) channel-cut monochromator (bending magnet source, Adone storage ring operating at 1.5 GeV, Frascati, Italy).

The paper is organized as follows: A complete description of the GNXAS fitting methodology is presented in Sec. II and details on the criteria for a correct statistical evaluations of the results are reported in Sec. III. In the successive sections a series of prototypical examples on diatomic (Sec. IV),

triatomic (Sec. V), diamond (Sec. VI A), and fcc (Sec. VI B) crystalline structures, will be reported. Section VII is devoted to the conclusions.

II. INVERSION OF THE STRUCTURAL INFORMATION

The GNXAS approach for EXAFS data analysis is based on a fitting procedure that optimizes the agreement between a model absorption signal $\alpha_{\rm mod}(E)$ and the experimental signal $\alpha_{\rm exp}(E_i)$.

The model absorption signal, as a function of the photon energy E, is given by

$$\alpha_{\rm mod}(E)=G(\sigma_r)*[J\sigma_0(E)[1+S_0^2\chi_{\rm mod}(E-E_0)]+\alpha_{bkg}(E)+\alpha_{\rm exc}(E)]. \quad (1)$$

Here $\chi_{\rm mod}$ is the actual EXAFS signal calculated according to the criteria described in I. S_0^2 is a constant reduction factor of the actual EXAFS intensity and accounts for an effective many-body correction to the one-electron cross section.[34] $\sigma_0(E)$ is a step function accounting for the atomic cross section of the absorption channel of interest. Above the edge it is a decreasing smooth function of the energy and can be modeled with an hydrogenic shape or using McMaster tables. The scaling factor J accounts for the actual surface density of the photoabsorber atoms. The background $\alpha_{bkg}(E)$ is a smooth polynomial spline accounting for the pre-edge region, and the post-edge contribution of all the absorption channels that opened at lower energies, and $\alpha_{\rm exc}(E)$ is instead a contribution in the post-edge region accounting for possible multielectron excitation channels. The spectrum is convoluted with an energy resolution function $G(\sigma_r)$ approximated as a Gaussian with standard deviation σ_r. σ_r can be determined by an independent fit of threshold features on a set of reference compounds and used as a fixed corrective parameter. Other broadening effects due to photoelectron mean free path and core-hole lifetime are included *ab initio* in the complex effective potential.

In our approach the edge jump J is determined by fitting the edge discontinuity and is gradually optimized as the other components of Eq. (1) are refined. Statistical noise and experimental reproducibility might, in principle, allow one to determine J with a relative error better than 10^{-3}. There is however an intrinsic uncertainty in the threshold shape of $\sigma_0(E)$ that reflects on J. Moreover for a given spectrum the inclusion of absorption contributions into $\alpha_{\rm exc}$ yields smaller J values. These effects bring an intrinsic uncertainty in J of even a few percent. The uncertainty on J reflects on S_0^2 since both scale the χ intensity. Therefore, in our approach, the parameter S_0^2 represents a phenomenological correction and accounts for both many-body effects and uncertainty in the correct jump normalization.

The account for the correct decay of σ_0 versus E, that normalizes the k dependence of the $\chi(k)$ intensity allows to fit absolute Debye-Waller factors.

A main characteristic of the GNXAS method is that a nonstandard atomic background function accounting for multielectron excitation thresholds can be adopted. In traditional methods the background is usually modeled as a smooth polynomial spline and subtracted prior to the analysis of the structural contribution. Many previous investigations from our group[35–37,18–20,38,39] have demonstrated that also in the case of embedded atoms the atomic background is often affected by the opening of double-electron excitation channels. The present theoretical approaches can be used to predict the double-electron excitation energies accurately whereas intensity and shapes are, for the moment, out of the reach of any suitable theory apart from the noble gases case.[40] However, the account of these effect can be performed at an empirical level as we have been proposing since 1988,[35] by means of a direct fitting of the raw absorption coefficient data with a model signal that includes both smooth background α_{bkg}, double-electron excitation contributions $\alpha_{\rm exc}$, and structural signal $\chi_{\rm mod}(k)$. Typical shapes of $\alpha_{\rm exc}$ account for autoionizing threshold resonances,[37] steplike edges, usually associated with shake-up channels,[41] and slope changes.[38,39] Specific examples are discussed elsewere.[35,18,19] The general relevance of the $\alpha_{\rm exc}(E)$ contribution has been widely emphasized.[42]

The need to refine the background component as the structural parameters are optimized has been emphasized by several other groups.[43–45] The background parameters are not physically correlated with the structural ones, and for this reason they are usually refined until a satisfactory background model is obtained and then fixed.

The natural energy scale on which the model signal has to be evaluated is the photon energy scale E. However, the χ signals are calculated on a convenient mesh E_t of appropriately spaced energy points. This theoretical energy scale has a zero corresponding to the level of the electrostatic potential at infinite distance, and an external parameter is required to match E_t with the experimental energy scale E. This corresponds to the position of $E_t=0$ on the actual photon energy scale and is indicated as E_0. Usually the E_0 value falls a few eV above the corresponding absorption threshold.

As a consequence of the finite electron mean free path the EXAFS signal is mostly sensitive to the short-range structure around the photoabsorber species. The relevant atomic arrangements are associated with the short-range peaks of the distribution functions $g_n(r)$. In many cases it is possible to model this short-range $g_n(r)$ shape as the sum of a a certain number of independent peaks, not necessarily Gaussian. Namely we can write,

$$4\pi r^2\rho g_2(r)=\sum_j n_j^{(2)}p_j^{(2)}(r),$$

$$8\pi^2 r_1^2 r_2^2\sin(\theta)\rho^2 g_3(r_1,r_2,\theta)=\sum_k n_k^{(3)}p_k^{(3)}(r_1,r_2,\theta), \quad (2)$$

where $n_j^{(2)}$ and $n_k^{(3)}$ are the degeneracies of the various configurations and the $p(\cdots)$ are normalized probability distributions describing the peak shapes. The left-hand sides of Eq. (2) represent the number densities for the actual configurations.

The previous assumption is straightforward for molecular or crystalline systems but also for disordered systems it can provide a reasonable description of the short-range order. If necessary, account for the contribution from the long distance $g_n(r)$ tails can be also taken.[24,29,46,27] In all cases, efforts should be performed to assess the reliability of the adopted model distributions. The comparison with structural

computer simulations performed with a realistic interatomic potential is usually found to be quite useful.

The configurational average of the $\chi(k)$ signal over these model distributions reduces to the sum of a certain number of oscillating contributions associated with each given peak. These can be calculated according to the prescription given in I, from the knowledge of the amplitudes, phases, and their derivatives with respect to the structural parameters. Let $A_j^{(n)}$ and $\psi_j^{(n)}$ be the amplitude and phases for the signal associated with peak j of the g_n. $A_j^{(n)}$ and $\psi_j^{(n)}$ have to be corrected for the effect of the shift of the average position and for the configurational average. These corrections, indicated as $A_j'(\lambda_1 \ldots)$ and $\psi_j'(\lambda_1 \ldots)$, will depend on a series of structural parameters including distances, angles, and mean-square vibrational amplitudes, hereafter indicated generically with λ_i. Their specific expression will depend on the order of the Taylor expansion spatial dimension, and peak model profile, as indicated in I. With the present notation the structural model contribution can be written as

$$\chi_{\mathrm{mod}}(E_t)=\sum_j n_j^{(2)}[A_j^{(2)}+A_j'(\lambda_1 \ldots)] \times \sin[\psi_j^{(2)}+\psi_j'(\lambda_1 \ldots)] + \sum_k n_k^{(3)}[A_k^{(3)}+A_k'(\lambda_1 \ldots)] \times \sin[\psi_k^{(3)}+\psi_k'(\lambda_1 \ldots)]+\cdots. \quad (3)$$

Summarizing, the final optimization procedure will involve a certain number of structural parameters plus two additional quantities S_0^2 and E_0. As is well known the uncertainty in S_0^2 induces uncertainty in coordination numbers, and similarly E_0 and the first-shell distance are also correlated. The uncertainties in the structural parameters can be, however, reduced and the parameter correlation avoided if S_0^2 and E_0 are calibrated on model compounds and fixed in the refinement of unknown compounds.

It is common practice to report and compare experimental and theoretical signals in k space since the oscillations are, to a good approximation, equally spaced on this scale. However, the correct definition of a k scale is not a trivial problem. We remark that using a complex energy-dependent exchange, the notion of photoelectron wave-vector modulus k requires more specifications. The physical k is complex and is intimately dependent on the approximations in the model for the potential. It is clear that the use of a theory-dependent k is extremely inconvenient. In the GNXAS method we have chosen to define a conventional k scale, according to common usage $k=\sqrt{2m(E-E_e)}/\hbar$, with respect to some threshold reference energy denoted E_e on the experimental energy scale. The actual choice of E_e, usually the inflection point of the absorption coefficient at threshold, does not affect the refinement procedure because it does not influence E_0. In the EXAFS comparison χ_{mod} is compared with χ_{exp} defined by the same background function starting from α_{exp} with an equation similar to Eq. (1). Due to the uniform oscillating behavior in k space the EXAFS signals are often also compared in R space after Fourier transformation. In the GNXAS approach this comparison in R space is performed by applying Fourier transformation to $\chi_{\mathrm{mod}}(k)$ and $\chi_{\mathrm{exp}}(k)$. We remind the reader that the fitting procedure is made on $\alpha_{\mathrm{mod}}(E)$ and no Fourier filtering is applied, k and R space representations are only used for graphical purposes and for the more convenient scales.

III. STATISTICAL EVALUATION OF THE RESULTS

The results of an EXAFS analysis can be affected by systematic errors originating from both experiment or approximations in the theory. The assessment of their magnitude, that is mainly limited by the accuracy of present theoretical approaches, is a fundamental step of the analysis. This can be accomplished by performing a series of comparisons on model compounds with known structure, and also by varying to some extent the free parameters in the theory, in particular, the muffin-tin radii used in the construction of the potential.[4] Examples of these kind will be discussed in the subsequent sections focused on the application of the GNXAS method. Current experience indicates that the magnitude of systematic errors is low and that very reliable structural results can be obtained from an EXAFS analysis based on theoretical calculations.

Under these circumstances any EXAFS report should be accompanied by a detailed analysis of the statistical errors due to random noise in the raw spectra. However, despite the wide applicative potential of the XAS, general procedures to estimate errors in the fitting parameters and to perform a statistical evaluation of the results are still not well established and are the subject of the present debate.

The importance of applying statistical tests to EXAFS analysis was pointed out by Joyner *et al.*,[47] in the framework of the EXCURVE package,[11] in particular emphasizing the importance of the correlation among structural parameters for a correct error evaluation, and indicating the possibility of using the F test in the assessment of hypotheses.

In a recent paper[48] the existence of a finite number of independent points N_{ind}, according to the finite k and R extension of the signals, has been emphasized. It has been suggested that N_{ind} is also a limit for the maximum number of parameters that can be fit to the spectrum. On the basis of these arguments, however it is not possible to tell which are the physical parameters that can be actually fit and which is the associated error. Moreover the definition of N_{ind} can provide only a rough estimate of this number.

Within the GNXAS approach we have adopted quite standard statistical procedures for nonlinear fitting problems originally developed in various physical context such as astrophysics[49] and high-energy physics.[50] We realized that some EXAFS error evaluation procedures suggested by other authors are at variance with these well established procedures, for this reason we feel quite important to describe our very general approach that we propose as a standard for EXAFS data analysis. Further details can be found elsewhere.[51]

In the GNXAS method the comparison between α_{mod} and α_{exp} is evaluated by means of a square residual function of the type

$$R(\{\lambda\})=\sum_{i=1}^{N}\frac{[\alpha_{\mathrm{exp}}(E_i)-\alpha_{\mathrm{mod}}(E_i;\lambda_1,\lambda_2,\ldots,\lambda_p)]^2}{\sigma_i^2}. \quad (4)$$

In Eq. (4) we explicitly indicated the p parameters $\{\lambda\}=(\lambda_1,\lambda_2,\ldots,\lambda_p)$ on which $\alpha_{\rm mod}$ depends. It is assumed that there exists a certain set of values for the parameters $\{\lambda\}=\{\lambda_r\}$ such that the theory reproduces exactly the true signal. It is also assumed that the experimental signal is only affected by random Gaussian noise with standard deviation σ_i for each E_i energy point around the true signal, that is

$$\alpha_{\rm exp}(E_i)=\alpha_{\rm mod}(E_i,\{\lambda_r\})+\xi_i, \tag{5}$$

where the expected value and covariance of the random noise ξ_i are $E\{\xi_i\}=0$ and $E\{\xi_i\xi_j\}=\delta_{ij}\sigma_i^2$. Under these condition the function $R(\{\lambda_r\})$ is a χ^2_N random variable on the space of the different realizations of the experimental noise.

A full statistical evaluation of the results can be performed according to the following four criteria.

(1) In the least-squares spirit, within a given choice for the structural model, the optimal values for the structural parameters are the set $\{\lambda\}=\{\bar\lambda\}$ such that the residual function $R(\{\bar\lambda\})$ is in a minimum.

(2) Because of the presence of p parameters, the $R(\{\bar\lambda\})$ function on the space of the possible realization of the experimental noise is better described by a χ^2_{N-p} random variable. Thus the statistical χ^2 test can be performed to check whether the actual value of $R(\{\bar\lambda\})$ is only due to residual noise or otherwise it contains unexplained physical information.

(3) The comparison between two different models (M_1 and M_2) for the structure, depending on p_1 and p_2 parameters, respectively, can be performed on the basis of the F test. Typical cases can be, for instance, the addition of a further n-body contribution, from M_1 to M_2, or the splitting of a shell into two. Let the respective residual minima be R_1 and R_2, then if both models are able to explain all of the signal one would expect the function

$$f=\frac{N-p_2}{p_2-p_1}\left(\frac{R_1}{R_2}-1\right) \tag{6}$$

to follow a $F_{p_2-p_1,N-p_2}$ distribution. The F test applied to f will tell in this case whether or not the reduction of the residual R obtained in the best model is actually large enough and not simply due to the increase of model parameters or to statistical fluctuations in the theory. The F test has been previously applied in EXAFS data analysis[47] especially by the users of the Daresbury EXCURVE package. Analogous results are commonly adopted in the context of the refinement of crystallographic data.[52]

(4) The statistical error on the best estimate of the parameters $\{\bar\lambda\}$ corresponds to the spread of the ensemble of $\{\bar\lambda\}$ values generated by the different possible realizations of the experimental noise ξ. In practice one has only one of these realizations available, but still the statistical theory provides specific criteria to determine the errors. Expanding to second order in λ and ξ the function $R(\{\lambda\})$ about the minimum, it is found that the actual $\{\bar\lambda\}$ values are displaced from the real value $\{\lambda_r\}$ by a linear function of the noise ξ. The ensemble of ξ values correspond to an ensemble of $\{\bar\lambda(\xi)\}$ values that, inserted into the $R(\{\lambda\})$ function, generate a random variable

$$R(\{\bar\lambda(\xi)\})=R(\{\bar\lambda\})+\chi^2_p, \tag{7}$$

that is a χ^2_p random variable (with p degrees of freedom) shifted by the value of R in the minimum. This allows to establish confidence intervals for the parameters, by applying the χ^2 test to Eq. (7), and therefore looking at regions in the parameter space for which $R(\{\lambda\})<R_{\rm min}+C$, with C depending on the confidence level of the analysis. Equivalently it can be shown that the probability of having certain $\{\lambda\}$ values in the space of the possible realization of the random noise is proportional to

$$P(\{\lambda\})\sim\exp\left(-\frac{1}{2}\chi^2(\{\lambda\})\right)=\exp\left(-\frac{1}{2}R(\{\lambda\})\right). \tag{8}$$

The region of parameter space delimited by the previous criteria, in the second-order approximation, is a p-dimensional ellipsoid. The covariance matrix defining the ellipsoid provides an insight into the correlation between the fitting parameters. Two-dimensional contour maps have long been used by the Daresbury group to view the correlations and error regions in the parameters space.[47] We point out that the constant C defining the confidence interval for a given confidence level depends on the number of fitting parameters p. This is a consequence of the multidimensional shape of the confidence interval, that has to be considered, in the simultaneous fit of several unknown parameters.[49,50]

In conclusion, the previous prescriptions of the nonlinear fitting theory provide definite answers to several important questions arising from the present EXAFS data analysis procedure.

A final aspect that remains to be clarified is the actual evaluation of the experimental noise σ_i entering Eq. (4). Excluding glitches σ_i can be modeled as a smooth function of the energy. In most cases $\sigma_i^2(E)$ can be directly estimated from the experimental spectrum, especially if it is oversampled in energy space, as shown by previous treatments.[53] We usually determine the average mean-square noise by fitting on the raw data polynomial functions in narrow intervals. These average values are successively interpolated with a smooth function and its inverse used as a weight function according to $1/\sigma_i^2$ in Eq. (4). In many practical cases a k^m weighting (with $m=2,3,\ldots$) results in a good approximation.

The previous statistical criteria are completely independent of the notion of $N_{\rm ind}$. This is not surprising because $N_{\rm ind}$ and the error evaluation are well separated problems. Our results are not in contrast with Stern's results,[48] in fact they provide the requested answers to questions that cannot be solved by the notion of $N_{\rm ind}$. In particular the error evaluation allows to identify the parameters that can be fit with sufficient statistical accuracy and those which are instead largely undetermined. There is nothing wrong, from the conceptual point of view, to perform a fit with $p>N_{\rm ind}$. A large number of parameters might still be not sufficient to explain the experimental data if the adopted model is not adequate. On the other hand the correct model usually is able to explain the experimental data with $p<N_{\rm ind}$. $N_{\rm ind}$ gives a rough estimate of the number of parameters that are likely to be fitted with statistical significance, therefore, if the fit is performed with $p>N_{\rm ind}$ it is likely that approximately $p-N_{\rm ind}$

parameters will result undetermined. The parameters can be easily identified with the error analysis according to the prescription (4) given above, this information cannot be obtained from the notion of $N_{\rm ind}$ only.

In the subsequent sections several examples of this kind of analysis will be presented, in particular, the possibility to fit parameters associated with three-body configurations will be demonstrated on the basis of solid statistical grounds. This is a fundamental step in the assessment of the EXAFS potential that is often put into question.

IV. DIATOMIC MOLECULES: Br_2

Diatomic molecules are the simplest systems predicted to present an EXAFS oscillation in their x-ray-absorption spectra. The Br_2 molecule in particular has been used, since the beginning, as a valuable reference[54] for the EXAFS theory. The GNXAS analysis of the Br_2 XAS spectrum has been the subject of previous papers[19,28] and we refer to those publications for typical levels of agreement obtained in k or R space.

The peculiar background due to the opening of several double-excitations channels, namely $KM_{4,5}$, $KM_{2,3}$, and KM_1, has been widely studied in molecular spectra of HBr and Br_2,[19] in brominated compounds[20] and in Br salts.[44,15,55]

In the case of both heteronuclear AB and homonuclear (with $B=A$) molecules the EXAFS signal is generated by a single two-body contribution and is given by

$$\gamma^{(2)}(A,B)=\chi_2^{ABA}+\chi_4^{ABABA}+\chi_6^{ABABABA}+\cdots . \quad (9)$$

While χ_2^{ABA} is certainly the dominant contribution very often the χ_4^{ABABA} gives a detectable correction. In some rare cases of very short bonds the $\chi_6^{ABABABA}$ and higher terms may also be important.[8] As previously discussed in I, due the large frequency difference between χ_2 and χ_4, it is preferable to simulate $\gamma^{(2)}$ signals with the MS sum if first-order Taylor expansions are used for the configurational average, otherwise a second-order Taylor expansion is recommended.

Here we would like to focus on typical problems in error evaluation and statistical significance of the fits. The best fit of the Br_2 spectrum, similar to that reported in Ref. 28 for the gas specimen was performed on $N=682$ points obtaining a residual χ^2 in the minimum of $\chi^2=722$. This is a case in which the theory has explained all of the structural signal present in the spectrum, in fact the 95% confidence level band includes a region of ± 74 around the expected value. The fit was performed with the four parameters R, σ^2, E_0, and S_0^2. Notice that according to Ref. 48 $N_{\rm ind}=2/\pi\times 16\times 1.2+2\sim 12$ is much larger than $p=4$. As usual R and σ^2 are mean and variance for the bond length distribution, that enter in the amplitude and phase displacement/damping corrections for the calculated signals. The structural results are reported in Table I, with their statistical errors associated with a 95% confidence interval. The statistical errors of the parameters are defined by the parameter space region where $R(\lambda)\leq\chi^2_{\rm min}+C$ where $\chi^2_{\rm min}=722$ (in this case) and C is a critical value of the χ^2_p random variable with $p=4$ (number of parameters) degrees of freedom, and 95% of confidence ($C=9.49$). This defines approximately a three-dimensional ellipsoidal surface in a four-dimensional space with a given covariance matrix from which the correlations among the parameters can be calculated. The correlations, shown in Table II, indicate that both R and E_0 and S_0^2 and σ^2 are highly correlated (≈ 0.86), as expected, mainly contributing to increase the errors in R and in σ^2, respectively. The contour plots associated with the two two-dimensional sections are shown in Fig. 1. Because the other correlations are small the maximum extension of the four-parameter confidence interval in the R and σ^2 directions can be accurately estimated from these curves. The errors reported in Table I account for this extension. The magnitude of statistical errors appears to be small as is usually the case for low noise spectra. The existence of extremely precise spectroscopic data for Br_2 allow one to check the reliability of the EXAFS results and to assess the magnitude of systematic errors due to approximations in the theory.

TABLE I. Results of the structural analysis of Br_2 EXAFS spectrum.

R (Å)	σ^2 (10^{-3} Å^2)	β
2.288(2)	2.0(1)	0.0(1)

As largely emphasized elsewhere,[28] at this level of refinement, it is important to compare exactly the same quantities, that are in this case the mean and variance of the Br-Br bond-length distribution at 300 K. These have for instance been calculated by Kuchitsu[56] for several diatomic molecules and for Br_2 the given values are $R_{sp}=2.2884$ Å and $\sigma^2=1.97\times 10^{-3}$ Å^2 in spectacular agreement with the present EXAFS result. In particular the systematic error in the average distance is, in this case, below 0.001 Å. This agreement indicates the intrinsic excellent accuracy of the presently available methods for EXAFS data analysis based on theoretical signal calculations.

A further interesting issue regards the possible EXAFS sensitivity to anharmonic effects in the bond-length distribution. This can be assessed releasing a fifth parameter $\beta=K_3/\sigma^3$ to account for a possible asymmetry in the distribution. The improvement in the residual from 722 to 700, is in this case too small, according to the F test, to accept the asymmetric model. If the β parameter is released the value $\beta=0.0(1)$ is found (Table I) where the error mainly arises from the correlation with the R parameter. This finding, in agreement with the result of the F test, indicates that EXAFS has not the sensitivity to probe the slight amount of asymmetry possibly present in the bond-length distribution at room temperature. The error in R quoted in Table I takes into account also the correlated uncertainty with the β parameter. The considerations drawn in this section extend with very

TABLE II. Statistical correlation between the parameters E_0, R, σ^2, and S_0^2 in the analysis of the Br_2 EXAFS spectrum. Only the upper off-diagonal terms of the symmetric matrix are indicated.

	E_0	R	σ^2	S_0^2
E_0		0.864	0.062	0.092
R			0.165	0.191
σ^2				0.865

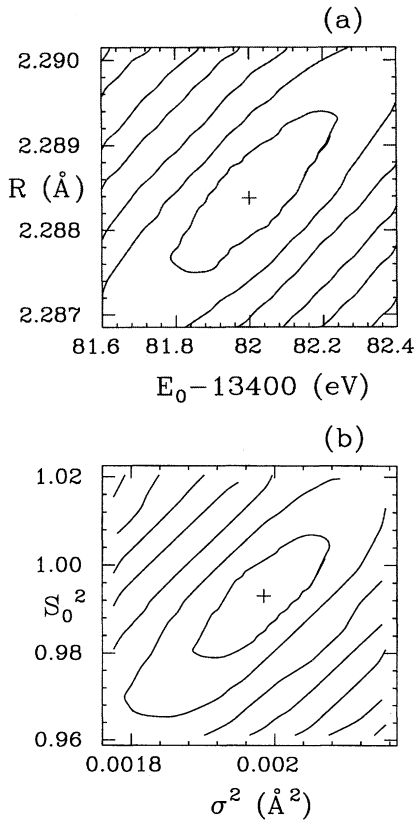

FIG. 1. Two-dimensional sections of the four-parameters confidence region for the fitting of the Br_2 EXAFS spectrum; (a) E_0-R correlations, (b) $\sigma^2-S_0^2$ correlations. The inner elliptically shaped curves represent the 95% confidence interval.

little modifications to the general problem of fitting the isolated first-neighbor contribution in EXAFS spectra.

V. TRIATOMIC MOLECULE: CS_2

In the general case the geometry of a triatomic molecule ABC will be parametrized by the lengths of the two real chemical bonds, say R_{A-B}, R_{A-C}, and by the enclosed angle θ_{B-A-C}. In the harmonic approximation six covariance matrix parameters are required, as described in I, to account for the thermal broadening, for a total of nine parameters. In the case of isosceles triangular molecules, with a $B\leftrightarrow C$ symmetry, like the SO_2 molecule, there will be only two geometrical and four covariance matrix parameters.

The EXAFS signal at an edge of the photoabsorber atom (say A) is given by the sum of two pair contributions $\gamma^{(2)}(A,B)$ and $\gamma^{(2)}(A,C)$ whose discussion is identical to the diatomic molecular case, and a single three-body contribution $\gamma^{(3)}(A,B,C)$. The existence of this $\gamma^{(3)}$ signal is the direct proof of the sensitivity of the XAS to triplet correlations. An electron-diffraction experiment on the same molecule would reveal oscillating contributions associated with the three pairs A-B, A-C, and B-C, but not with the simultaneous position of the three atoms. So in this case actually EXAFS and electron diffraction on gas specimens provide complementary information. In the Gaussian approximation for the bond vibrations, electron diffraction is sensitive to average distances and variances for the three bonds in the system, that are six independent parameters. EXAFS instead provides, in principle, information also on the correlations between the vibration of all three bonds.

The $\gamma^{(3)}(A,B,C)$ signal is calculated according to the criteria described in I either with the appropriate MS expansion or directly with the continued-fraction expansion approach that presents several computational advantages. The configurational average can be performed using first-order Taylor expansion expressions that are accurate enough.

A special case is that of linear A-B-C molecules. Examples are the S=C=O (carbonylsulfide) and the S=C=S (carbon disulfide), that can be studied at the S K edge. The latter will be considered in the present paper.

Looking at the real frequency content of the spectrum of an A-B-C linear molecule, it is clear that the low-frequency A-B contribution already constrains the two structural parameters R_1 and σ_1^2. The other contribution $\gamma^{(2)}(A-C)$ and the three-body signal $\gamma^{(3)}(A-B-C)$ have similar leading frequencies (R_1+R_2) and both contribute to the second peak in the Fourier transform with an effective shell signal $\eta^{(3)}(A-B-C)=\gamma^{(3)}(A-B-C)+\gamma^{(2)}(A-C)$. Due to the focusing geometry the effect of the C atom on the EXAFS is strongly enhanced.

The effect of the configurational average on the collinear case deserves a thorough discussion. The average positions of the atoms are, by definition, aligned, however, in a real vibrating system the probability of finding exactly a linear configuration ($\theta=180°$) vanishes like $\sin(\theta)$ as the spherical volume element. For such an extremal condition the Gaussian model has to satisfy the previous limiting conditions and obvious symmetry constraints. A general expression for the probability density in terms of the three coordinates r_1, r_2 (indicated with r), and θ will be

$$f(r,\theta)=\frac{1}{2\pi\sqrt{\mathrm{Det(m)}}}\exp\left(-\frac{1}{2}(r,m^{-1}r)\right)\frac{(180-\theta)}{\delta_\theta^2}\times\exp\left(-\frac{(\theta-180)^2}{2\delta_\theta^2}\right),\quad 0\leq\theta\leq 180. \tag{10}$$

In this equation the quadratic form $(r,m^{-1}r)$ involves only the two distance coordinates and the covariance matrix m is a 2×2 matrix in the distance subspace. The distance and angular distributions are actually factorized. The reason is that the existence of nonvanishing cross terms of the type $r_i(\theta-180)$ would imply a change of the distance probability according to the sign of the angle fluctuation around 180, which, on the other hand, corresponds to the same displacement. The total harmonic model distribution depends on six parameters; two average parameters R_1, R_2, and four covariance matrix parameters σ_1^2, σ_2^2, ρ_{12}, and δ_θ^2. In the case of additional equivalence of the two bonds (like in CS_2) these reduce to four, one average parameter R_1, and three covariance matrix parameters σ_1^2, $\rho_{1,1'}$, and δ_θ^2, Notice that in both cases R_1 and σ_1^2 are already constrained by the first-shell contribution whereas the others are eventually defined by the analysis of the second-shell contribution.

The angular distribution has a maximum for $\theta_M=180-\delta_\theta$, the second moment about 180° of θ is $2\delta_\theta^2$

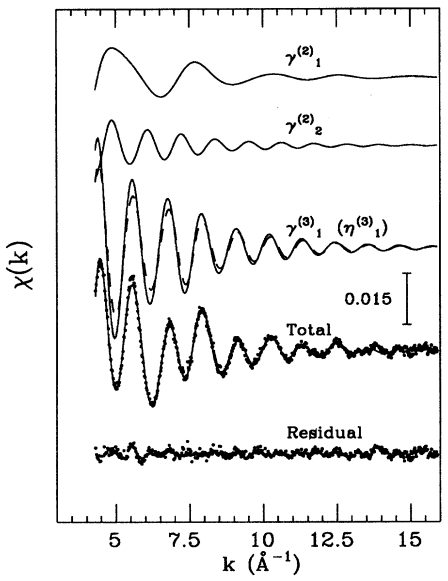

FIG. 2. Analysis of the CS_2 spectrum at the S K edge. The various curves from top to bottom refer to the two-body S=C contribution $\gamma_1^{(2)}$, the two-body S$\cdots$S contribution $\gamma_2^{(2)}$, and the three-body S=C=S contribution $\gamma_1^{(3)}$. On the same baseline the effective second-shell signal $\eta_1^{(3)}$ is reported (dashed curve). The lower curves represent the comparison between total model and experimental signals (dots) and the residual containing only statistical noise.

and the variance is $\sigma_\theta^2=(4-\pi)/2\delta_\theta^2$. We point out that for large fluctuations the disordered linear configuration can be confused with a case of disorder around a bent average configuration. The EXAFS determination of geometrical parameters in linear cases has been previously applied by our group.[32,22] Recent papers by other authors[15] have treated linear configurations and deviations from linearity in ionic compounds.[16,57]

The actual configurational average of the three-body signal is performed including second-order derivatives with respect to the angle fluctuations,[32] that is the first nonvanishing term. This has been recently also pointed out by other authors.[57] The actual average of the signal over the distribution function is performed using the expression

$$\langle\chi(k)\rangle\sim\Im A_0\exp(i\psi_0)\left[1+\frac{i}{A_0}(A_1,m\psi_1)+\frac{1}{A_0}A_2^\theta\delta_\theta^2\right]\times\exp\left[-\frac{1}{2}(\psi_1,m\psi_1)\right](1-i\psi_2^\theta\delta_\theta^2)^{-1},\qquad(11)$$

where the quadratic forms are limited to the distance coordinates and A_2^θ and ψ_2^θ indicate the second derivatives of amplitude and phase of the signal with respect to the angle, calculated at $\theta=180°$.

The spectrum of the CS_2 molecule was recorded at the PULS-EXAFS beamline in Frascati. The analysis of the structural signal is presented in Figs. 2 and 3. In Fig. 2 we show the various contributions in k space. From top to bottom are reported: $\gamma_1^{(2)}$ (S-C), $\gamma_2^{(2)}$ (S-S), $\gamma_1^{(3)}$ (S-C-S) [$\eta_1^{(3)}$ (S-C-S) as a dashed line on the same baseline]. The importance of including MS effects is epitomized by this linear molecular case. MS accounts for over 60% of the signal, the effective second-shell signal $\eta_1^{(3)}$, is dominated by the three-body contribution. More precisely $\eta_1^{(3)}$ results slightly weaker than $\gamma_1^{(3)}$ because the $\gamma_2^{(2)}$ signal is in opposition of phase. The contributions of the various signals in the Fourier transform is reported in Fig. 3. The agreement between calculated and experimental spectra is satisfactory.

In the fitting of the CS_2 spectrum account was taken for the presence of the KL edge using empirical shapes as reported in previous papers.[35,18] The importance of the KL edge in S compounds has been largely emphasized elsewhere.[37]

The statistical evaluation of the errors has been performed following present criteria. According to Ref. 48 the number of independent EXAFS points, for $\Delta k=12.5$ Å^{-1} and $\Delta R\approx4$ Å (the R-space interval containing signal) is $N_{\rm ind}\approx34$. In our spectrum the number of experimental points is $N=567$, while a perfect fit is obtained with only six parameters ($p=6$), four geometrical, E_0 and S_0^2. The residual χ^2 of the fit is $\chi^2\simeq618$ indicating that the model is able to explain satisfactorily the experimental signal. This is, in general, not the case if a wrong model is assumed or if MS is neglected. In the CS_2 case, for instance, the best fit excluding the three-body contribution is only able to reach a residual χ^2 of about 12 000 with completely unphysical parameters.

The 95% confidence interval for the statistical errors in the six-dimensional parameter space were obtained with the intersection $R(\lambda)=\chi^2_{\rm min}+C$ where C was in this case the critical value of the χ_p^2 random variable for $p=6$, that is

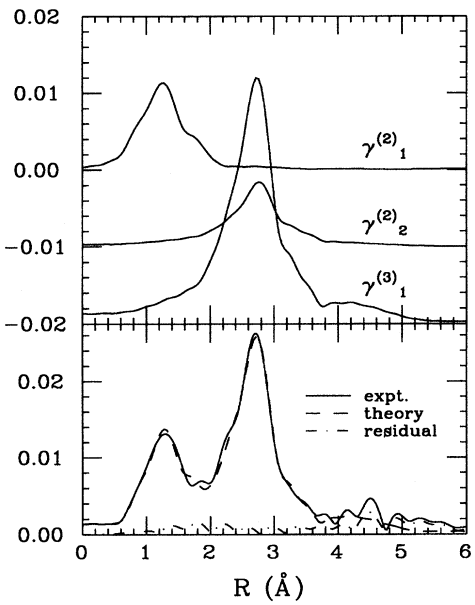

FIG. 3. Magnitudes of the Fourier transforms of the signals reported in Fig. 2, performed in the interval $k=4.3-15.9$ Å^{-1}. The signal is dominated by the $\gamma_1^{(3)}$ contribution. In the lower part of the figure the comparison between experiment, theory, and residual is reported.

TABLE III. Results of the structural analysis of the CS_2, S K-edge EXAFS spectrum.

R (Å)	σ^2 (10^{-3} Å^2)	δ_θ^2 ($^{\circ 2}$)	$\rho_{1,1'}$
1.547(2)	1.6(4)	30(10)	-0.4(2)

$C=12.6$. A summary of the optimal values for the four structural parameters is reported in Table III. The statistical error for the C=S bond length R is found to be ± 0.002 Å, however, the optimal value is about 0.01 Å lower than the electron-diffraction determination,[58] suggesting the presence of a small systematic error possibly due to the presence of a slight asymmetry neglected in the model.

The most interesting results, however, concern the vibrational parameters for which the EXAFS sensitivity was not so obvious. In Fig. 4 two contour maps associated with the σ^2-S_0^2 and δ_θ^2-$\rho_{1,1'}$ parameter spaces are shown. They indicate the presence of a well defined minimum in the parameter subspace affecting the three-body contribution only. The two C=S bonds are found to vibrate in an anticorrelated way $\rho_{1,1'}=-0.4(2)$, while the bond-angle fluctuations amount to $\delta_\theta^2=30(10)^{\circ 2}$. The resulting variance of the S-S bond is $1.9(2)\times 10^{-3}$ Å^2. These results demonstrate the possibility of deriving information on the vibrational correlations of three-body units by fitting EXAFS contributions in the framework of our data-analysis method.

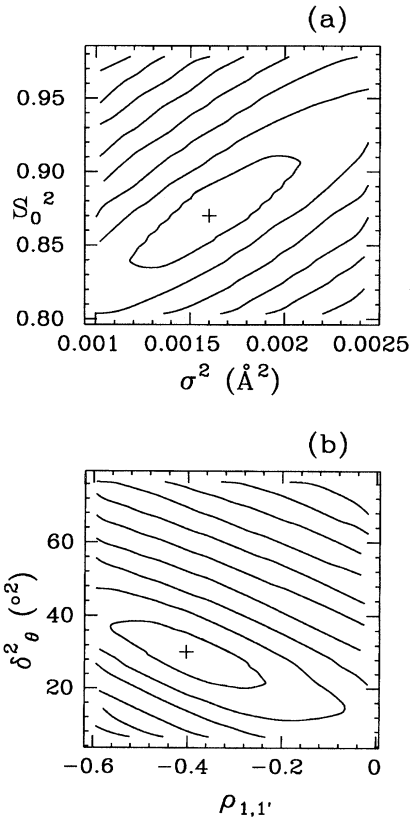

FIG. 4. Correlation maps between several fitting parameters of the CS_2 spectrum at the S K edge. (a) $\sigma^2 \leftrightarrow S_0^2$ plane, (b) $\rho_{1,1'} \leftrightarrow \delta_\theta^2$ plane. The inner elliptically shaped curves represent the intersection with the 95% confidence interval.

VI. SIMPLE CRYSTALS

The GNXAS method can be applied in a straightforward manner to simple crystalline structures. Applications to c-Ge (diamond) and c-Pd (fcc) are reported in this section. In both cases the strongest EXAFS contribution comes from the first shell of neighbors which are directly bonded. Successive contributions include higher shells and three-body configurations formed by two first-neighbor bonds linked at different angles.

The three-body configurations are, in general, characterized by two distances R_1 and R_2 and the enclosed angle θ, the same geometry gives rise to different signals associated with different photoabsorber positions. In our convention position 1 corresponds to the vertex between the two short bonds, position 2 is at the end of the first bond (with length R_1) and position 3 is at the end of the second bond. The EXAFS contribution corresponding to these positions will be referred to as $\gamma_{p1}^{(3)}$, $\gamma_{p2}^{(3)}$, and $\gamma_{p3}^{(3)}$, respectively. These signals are not independent since they are simultaneously modified according to actual equilibrium position and vibration parameters. Their degeneracy equals the triangle degeneracy per atom in the structure. In the case of isosceles or equilateral triangles some of the previous signals coincide and they can be calculated only once with the appropriate multiple degeneracy. Notice that these contributions include MS to any order. The third side of the triangle (if not equilateral) will correspond to a higher coordination shell. In order to limit the number of geometrical parameters and avoid redundancy, the related two-body signal $\gamma_{n\geq 2}^{(2)}$ is calculated on the corresponding three-body structural configuration. The coordination number associated with this shell is equal or less than twice the triangle degeneracy. In fact, due to the connectivity of the network, several distinct triangles can have a common long distance vertex. The sum of the pair and three-body contributions, that is, the effective higher shell signal, is as usual defined by

$$\eta^{(3)}=\gamma_n^{(2)}+\gamma_{p1}^{(3)}+\gamma_{p2}^{(3)}+\gamma_{p3}^{(3)}, \tag{12}$$

all signals are in fact associated with the same geometry and are oscillating contributions in k with similar leading frequencies.

In the following subsection we will demonstrate with explicit examples that

(1) It is important to account for triangular MS effects in simple crystalline structures.

(2) The correlated vibration of the units can be actually determined by EXAFS with statistical significance.

A. Diamond: c-Ge

The diamond structure is common to several crystalline semiconductors like c-Si and c-Ge, but also III-V and II-VI compounds to which present considerations extend with little modifications accounting for the presence of two atomic species. The structural analysis of the shortest two-body and three-body configurations is reported in Table IV. The dis-

TABLE IV. Pair and triplet contributions in the diamond structure. The distances are reported in units of the nearest-neighbor distance R, the angles are in degrees. The degeneracy (Deg.) is specified for each configuration. The photoabsorber position for the triplet configurations is also specified (Pos.). Position 1 corresponds to the vertex between the two short bonds, position 2 is at the end of the first bond (with length R_1) and position 3 is at the end of the second bond.

Peak	R_1/R	R_2/R	θ (°)	Deg.	Pos.	$R_{\text{path}}/2R$
Pair distribution						
1	1			4		1
2	$\frac{2}{3}\sqrt{6}$			12		1.633
3	$\frac{1}{3}\sqrt{33}$			12		1.915
4	$\frac{4}{3}\sqrt{3}$			6		2.309
5	$\frac{1}{3}\sqrt{57}$			12		2.517
6	$2\sqrt{2}$			24		2.828
7	3			16		3
8	$\frac{4}{3}\sqrt{6}$			12		3.266
Triplet distribution						
1	1	1	109.47	6	1	1.816
				12	2	1.816
2	1	$\frac{2}{3}\sqrt{6}$	90.00	24	1	2.274
				24	2	2.274
				24	3	2.274
3	$\frac{2}{3}\sqrt{6}$	$\frac{2}{3}\sqrt{6}$	60.00	24	1	2.449
4	1	$\frac{2}{3}\sqrt{6}$	144.74	12	1	2.575
				12	2	2.575
				12	3	2.575

tance unit is the first-shell distance $R=a\sqrt{3}/4$, a being the cubic lattice parameter. The last column reports the equivalent geometrical length associated with the corresponding EXAFS signal in R space $R_{\text{path}}/2R$.

The diamond structure is sufficiently open to allow a gradual onset of the importance of higher-order MS terms. Present analysis is limited to the third-shell frequency range and therefore includes: (a) first-shell contribution, (b) combined second-shell and main three-body contribution, and (c) third-shell contribution at the two-body level.

The main triangular configuration in the diamond structure is isosceles with two first-shell bonds joined, in the center of a tetrahedron, by a 109.47° angle. The main MS signals associated with this triangle have been widely discussed in early MS applications.[59] In the GNXAS analysis this configuration is counted with a degeneracy of 6 (six triangles per atom). Due to symmetry it generates a $\gamma_{p1}^{(3)}$ signal with degeneracy of 6, and a $\gamma_{p2}^{(3)}$ with double degeneracy of 12. The second-shell contribution $\gamma_2^{(2)}$ associated with the third side of the triangle has, in this case, a coordination number of 12.

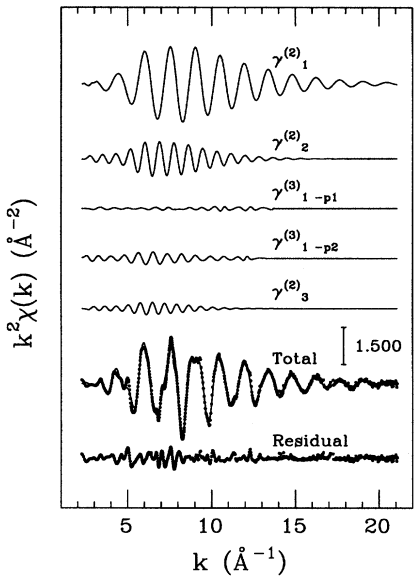

FIG. 5. Best fit of the c-Ge spectrum at 294 K, the various theoretical $k^2\chi(k)$ signals corresponding to pair and triplet contributions are reported as continuous lines. In the lower part of the figure, the comparison between total theoretical signals (solid line) and experiment (dots), and the residual experimental data are reported.

The analysis of the diamond structure can be extended to higher-shells involving higher order terms, however, in the present example we will limit the analysis to the third-shell contribution treated at the two-body level. Weak MS corrections, are expected for this distance range from the second three-body configuration (Table IV). We believe that the presentation is in this way clearer still representing an advance with respect to the EXAFS data analysis usually performed at the Ge K edge.

The experimental spectrum of high-purity Ge powder at room temperature (294 K) was collected at LURE at the D42 beamline equipped with a channel-cut Si (331) monochromator. The powder was finely ground to submicrometric size to avoid nonlinear reductions of the sample absorption coefficient and purified *in situ* by heating above the melting point.[27]

The best fit was performed by varying a total of 11 parameters: E_0, S_0^2, (R_1, σ_1^2, β_1) for the first-shell distribution, (θ, σ_θ^2, $\rho_{1,\theta}$, $\rho_{1,1'}$) for the three-body main contribution, and (R_3, σ_3^2) for the third shell. The first-shell asymmetry parameter β_1 was found to be close to zero indicating validity of the Gaussian approximation in a wide temperature range.[27] The actual intensity of the various contributions to the signal is shown in Fig. 5. The curves, from top to bottom refer to the first shell $\gamma_1^{(2)}$ signal, the second shell $\gamma_2^{(2)}$ signal, actually calculated on the triangular configuration associated with the next $\gamma_{p1}^{(3)}$ and $\gamma_{p2}^{(3)}$ signals, and finally the third shell $\gamma_3^{(2)}$ signal. The successive curve is the total theoretical signal (solid line) compared with the experimental spectrum (dots); the residual signal is also reported (bottom spectrum) and contains mainly higher-frequency contributions while in the high-k range it is dominated by

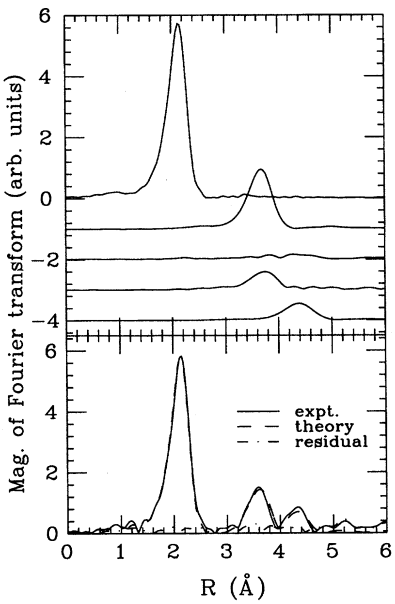

FIG. 6. Best fit of the c-Ge spectrum at 294 K; magnitude of the Fourier transforms of the successive contributions calculated with a k^2 weight in the 2.2–21.1 Å^{-1} range. In the lower part of the plot the comparison between total theoretical signals and experiment is reported. The agreement in the first- and second-shell peaks is excellent.

experimental noise only. Notice the agreement between experimental and theoretical spectra, obtained up to the end of the measured spectrum $k=21$ Å^{-1}.

The corresponding magnitudes of the Fourier transforms of the signals are shown in Fig. 6. Notice the agreement obtained in the fitted frequency region (especially in the first and second-shell peaks). From the inspection of Figs. 5 and 6 it is clear that the MS $\gamma^{(3)}$ contributions provide a detectable and important contribution in the 3.5–4 Å frequency range. This was already observed in the very similar c-Si case,[59] but in the analysis of c-Ge and related systems the MS contributions have been always neglected. In the c-Ge case the $\gamma^{(3)}$ contributions are less important than is c-Si, but they still account for the 30% of the signal in the second-shell peak range, and cannot be neglected. Because of the opposition of phase between the $\gamma_2^{(2)}$ and the $\gamma_{p2}^{(3)}$ signal, the total effective second-shell contribution $\eta^{(3)}$ is slightly weaker than the $\gamma_2^{(2)}$ pair contribution. For this reason the spectrum can be reasonably fitted with the $\gamma_2^{(2)}$ signal only, but, in this case the σ_2^2 parameter results over-estimated. In the present GNXAS analysis, that includes $\gamma^{(3)}$ signals, the σ_2^2 parameter is not fitted directly, however, it can be derived from the other vibrational parameters using, for an isosceles (noncollinear) triangle, the formula

$$\sigma_2^2=(1-\cos\theta)\sigma_1^2(1+\rho_{1,1'})+2R_1\sin\theta\rho_{1,\theta}\sqrt{\sigma_1^2\sigma_\theta^2}+\frac{R_1^2\sin^2\theta}{2(1-\cos\theta)}\sigma_\theta^2 \quad (13)$$

obtained by calculating the variance of the random variable $R_2(R_1,R_{1'},\theta)$.

TABLE V. Results of the structural analysis of c-Ge EXAFS spectrum at 294 K.

Shell	R (Å)	σ^2 (10^{-3} Å^2)	β
I	2.449 (2)	3.6(1)	0.0(1)
II[a]	4.013 (5)	10(1)	
III	4.74 (2)	17(2)	
Three-body configuration			
θ (°)	σ_θ^2 (°^{2})	$\rho_{1,1'}$	$\rho_{1,\theta}$
110.1(2)	14(2)	-0.35(15)	-0.10(5)

[a]Derived from the three-body parameters.

In this c-Ge case, where higher-frequency contributions have been neglected, the residual function largely exceeds the expected value for the given statistical noise. This is clear looking at Figs. 5 and 6 where there is an high-frequency residual not explained by the model spectrum. This, however, has not particularly dramatic consequences on the statistical evaluation of the results, in fact, the minimum of the residual function results simply translated by a residual χ_r^2 associated with the high-frequency components. Error confidence interval in the 11-dimensional parameter space can still be estimated by the surface defined by the equation $R(\lambda)=R_{\min}+C$ where $C=19.7$ is the critical value of the χ_p^2 random variable with $p=11$ and 95% confidence level.

The optimal values for the structural parameters are reported in Table V. The correlations between E_0, S_0^2 and the first-shell parameters are very similar to the ones reported for the previous molecular examples and for this reason the results will be omitted. More interesting, in this case, is the possibility to actually fit the parameters associated with the triangular configuration. In Fig. 7 we report correlation maps between $\rho_{1,1'}$, σ_θ^2 and $\rho_{1,\theta}$, $\rho_{1,1'}$. These maps clearly indicate, not only that a well defined minimum exists in the three-body parameter subspace, but also that the parameters can be determined with high accuracy. The average configuration and correlated vibration of this fundamental Ge-Ge-Ge triangle is described as follows. The average bond angle is found to be slightly larger than the tetrahedral one, 110.1(2)°, however the standard deviation of the angular vibration amounts to nearly 4° and therefore the bond-angle distribution is well centered around the geometrical value. The departure from the exact value might indicate the presence of a slight anharmonicity that is not accounted for by the model distribution. The two adjacent first-neighbor bonds are found to vibrate in a slightly anticorrelated way $\rho_{1,1'}=-0.35(15)$ and this is not surprising in light of the vibrational properties of the solid. Similarly the bond and adjacent angle vibrations are found to be slightly anticorrelated, $\rho_{1,\theta}=-0.10(5)$, that is, the bond angles expand when the bond lengths tend, on the average, to contract slightly.

The fitted value for the Ge-Ge average bond length is found to be in agreement with the the known average lattice spacing in c-Ge. This again indicates the absence of substantial systematic errors due to approximations in the theory. The case of c-Ge epitomizes the level of insight that can be gained with the present data-analysis method on simple crystalline systems.

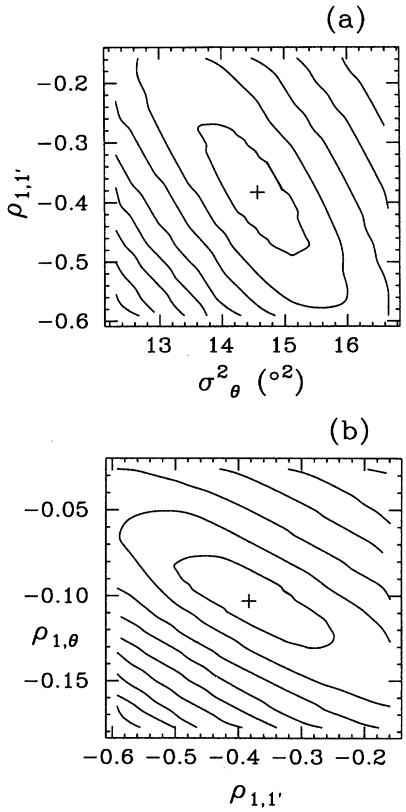

FIG. 7. Correlation maps between the three-body parameters for the best fit of the c-Ge spectrum at 294 K. (a) $\rho_{1,1'} \leftrightarrow \sigma^2_\theta$ plane, (b) $\rho_{1,\theta} \leftrightarrow \rho_{1,1'}$ plane. The inner elliptically shaped curves represent the 95% confidence interval.

B. fcc crystals: c-Pd

The fcc structure is representative of several transition metals. The structural analysis of the corresponding two-body and three-body configurations is reported in Table VI. The first-shell distance unit is $R=a/\sqrt{2}$, where a is the cubic lattice parameter. Looking at the geometrical frequency of the successive contributions it is clear that the first three-body term starts contributing at the frequency 1.5 times that of the first shell. For this reason, while the first-shell signal is completely isolated, several pair and triplet contributions overlap starting from the second-shell signal. The shortest four-body contributions have a frequency of twice the first-shell signal, but they are in any case expected to be small due to the large scattering angles involved. Therefore, it is expected that, from the second-shell to the fourth-shell region included, the spectrum can actually be interpreted in terms of pair and triplet contributions only.

The structural contributions, signals, and associated parameters, included in the present analysis, are

(1) The first-shell $\gamma_1^{(2)}$ signal modeled as a Γ distribution[27] with parameters R_1, σ_1^2, and β_1 corresponding to average, variance and skewness (dimensionless) of the bond-length distribution.

(2) The second-shell signal $\gamma_2^{(2)}$, treated as the one above, depending on parameters R_2, σ_2^2, and β_2. Is is expected that $\sigma_2^2 > \sigma_1^2$ due to less correlated thermal motions.

TABLE VI. Pair and triplet contributions in the fcc structure. The distances are reported in units of the nearest-neighbor distance R, the angles are in degrees. The degeneracy (Deg.) is specified for each configuration. The photoabsorber position for the triplet configurations is also specified (Pos.).

Peak	R_1/R	R_2/R	θ (°)	Deg.	Pos.	$R_{\text{path}}/2R$
1	1			12		1
2	$\sqrt{2}$			6		$\sqrt{2}$
3	$\sqrt{3}$			24		$\sqrt{3}$
4	2			12		2
5	$\sqrt{5}$			24		$\sqrt{5}$
6	$\sqrt{6}$			8		$\sqrt{6}$
1	1	1	60	24	1	1.5
2	1	1	90	12	1	1.707
				24	2	1.707
3	1	1	120	24	1	1.866
				48	2	1.866
4	1	1	180	6	1	2
				12	2	2
5	1	$\sqrt{2}$	90	24	1	2.073
				24	2	2.073
				24	3	2.073
6	1	$\sqrt{3}$	73.22	48	1	2.232
				24	3	2.232
7	1	$\sqrt{2}$	135.00	24	1	2.325
				24	2	2.325
				24	3	2.325

(3) The shortest triplet contribution that originates from equilateral triangular configurations. The triangle degeneracy is 8. In this peculiar geometry all of the atoms are equivalent and there is a single $\gamma^{(3)}$ signal with degeneracy 24. The natural coordinates are the three equivalent bond distances. The equilibrium geometry is univocally defined by the previously introduced parameter R_1. The vibrational damping in the Gaussian approximation is defined by the covariance matrix depending on two parameters σ_1^2 (already introduced) and the covariance $\sigma_{1,1'}^2$ that describes the correlated variance between the vibrations of neighboring first-neighbor bonds. The correct account of the equilateral triangles requires only the addition of a single structural parameter in the fit.

(4) The next three-body contributions in parameter space are the isosceles triangles with two first-neighbor bond sides and vertex angles of either $\theta_{90}=90°$ or $\theta_{120}=120°$. The analysis of these structures is similar to the fundamental triangle in the diamond lattice. Notice that the long bond of the triangles correspond to the second and third shells of the fcc structure, with equilibrium distances of a and $a\sqrt{3}/2$, respectively. The orthogonal triangles have a degeneracy of 12 but the corresponding second-shell coordination number is only 6. Similarly the 120° triangles have a degeneracy of 24, while the third-shell coordination number is 24. In both cases the reduction is due to the large network connectivity. Due to the weakness of the three-body orthogonal contributions, in the present case, the second shell is introduced at the pair

level. Instead the 120° triangle and corresponding third shell are included as a three-body contribution. The equilibrium position is defined by the structural parameters R_1 and θ_{120} (only the last is a new one if it is not fixed), while the covariance matrix parameters are σ_1^2, σ_θ^2, $\rho_{r\theta}$, $\rho_{r,r''}$ (only three new ones).

(5) Finally, an important three-body contribution originates from the degenerate triangle between three aligned first neighbors. There are six of these configurations per atom and therefore six $\gamma_{p1}^{(3)}$ signals and 12 $\gamma_{p2}^{(3)}$ signals. The third side of the triangle corresponds, in this case, to the fourth coordination shell ($\gamma_4^{(2)}$ signal). This is a well-known case in which MS contributions are particularly strong. The effective fourth-shell signal $\eta^{(3)}$ has a regular oscillating behavior and is relatively intense. Due to the collinearity of the equilibrium position the model distribution for the coordinates, previously discussed in the CS_2 case Eq. (10), vanishes for $\theta=180°$. This contribution requires only two new fitting parameters: the angle distribution width parameter δ_θ^2, and the bond–next-collinear-bond correlation $\rho_{r,r'''}$.

We remark, as a general comment, that the correct treatment for an isosceles three-body contribution requires only two more parameters than those corresponding to a shell addition. For collinear paths no additional parameters are required going from a coarse single-scattering approximation to the exact account of the three-body MS effects. In practice, contrary to what is commonly believed, the inclusion of several three-body contributions can be performed without requiring an uncontrolled growth of the number of parameters.

A spectrum of crystalline Pd has been collected at the LURE laboratories D44-XAS4 beamline Si(311) monochromator, in the framework of an experiment on high-temperature phases of Pd. A room-temperature spectrum at 296 K will be considered in the present analysis.

The fitting was performed with a total of 15 parameters (13 structural) divided as follows: first shell R, σ^2, β_1; second shell R_2, σ_2^2, β_2; 60° triangle, $\rho_{r,r'}$; 120° triangle and third shell, θ_{120}, $\sigma_{\theta 120}^2$, $\rho_{r\theta}$, $\rho_{r,r''}$; 180° triangle and fourth shell, δ_θ^2, $\rho_{r,r'''}$, and finally E_0 and S_0^2.

The result of the fitting is shown in k space in Fig. 8 and the corresponding Fourier transforms are reported in Fig. 9. The agreement between theory and experiment is remarkable in the whole frequency range. The values for the structural parameters are reported in Table VII including the correlated statistical errors determined as usual (Sec. III).

In line with the main aim of the paper we will again enter in the discussion of the error evaluation in some detail. Let us start with the first-shell parameters, we found $R=2.747(3)$ Å where the statistical error includes the correlation with the E_0 parameter, only. Similarly we found for $\sigma^2=5.6(4)\times10^{-3}$ Å^2 including correlation with S_0^2. The contour map in the σ^2-S_0^2 parameter space is shown in Fig. 10(a). The R value is found to be slightly shorter than the crystallographic Pd-Pd distance $a/\sqrt{2}=2.751$. If the additional parameter β describing the asymmetry of the peak distribution is floated, it refines to negligible asymmetry $\beta=0.0(1)$, however, increased correlation increases the statistical error in the R determination, resulting $R=2.747(5)$ Å. These findings are in line with with previous EXAFS

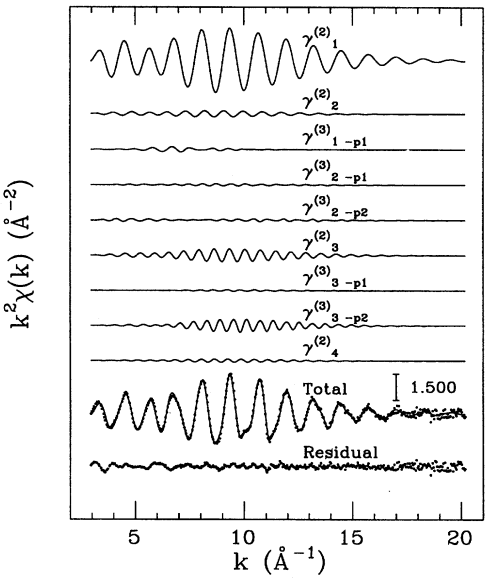

FIG. 8. Best fit of the Pd foil spectrum at 296 K, the various theoretical $k^2\chi(k)$ signals corresponding to pair and triplet contributions are reported as continuous lines. In the lower part of the figure, the comparison between total theoretical signals (solid line), experiment (dots), and the residual experimental data are reported.

studies on Pd foils[60] made using the FEFF code. The comparison of the σ^2 values between GNXAS and FEFF results is also quite good. Our value $5.6(4)\times10^{-3}$ Å^2 is only slightly smaller than both the reported value 6×10^{-3} Å^2 (Ref. 60) and another determination (6.3×10^{-3} Å^2) obtained by other

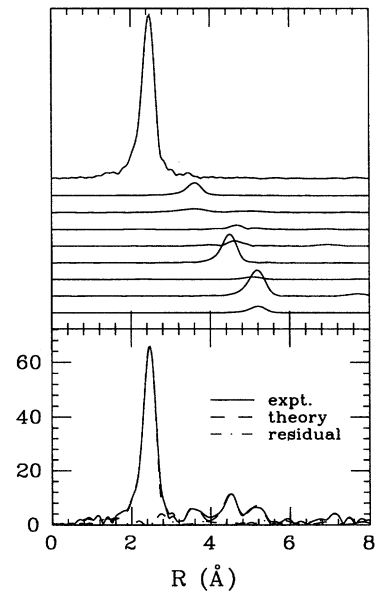

FIG. 9. Best fit of the Pd foil spectrum at 296 K; magnitude of the Fourier transforms of the successive contributions calculated with a k^3 weight, the order is the same of Fig. 8. In the lower part of the plot the comparison between total theoretical signals and experiment is reported.

TABLE VII. Results of the structural analysis of Pd foil at 296 K. The parameters for the three triplet configurations correspond to peaks 1, 3, and 4 in Table VI.

Shell	R (Å)	σ^2 (10^{-3} Å^2)	β
I	2.747(5)	5.6(4)	0.0(1)
II	3.86(2)	10(3)	-.1(3)
III [a]	4.77(1)	8.5(10)	
IV [a]	5.49(1)	9.8(10)	
Three-body configurations			
θ (°)	σ^2_θ (°^{2})	$\rho_{1,1'}$	$\rho_{1,\theta}$
60(f)		$\geqslant$0.0	
120.7(4)	$\leqslant$10	-0.2(4)	0.0(3)
180(f)	$\leqslant 10^{b}$	-0.1(3)	

[a]Derived from the three-body parameters.
[b]Value corresponds to δ^2_θ in Eq. (10).

authors.[61] The larger value obtained in previous studies is probably due to $S_0^2=1$ constraint adopted. We found instead a better overall agreement with a lower value around 0.84, that should account for the incoherent cross section that contributes to the jump but not to the signal. Theoretical estimates for the $\sigma^2(T)$ for Pd can be obtained scaling previously published calculations for Cu.[62] Due to the similarities in the vibrational properties of Pd and Cu,[63,64] scaling factors in temperature and variance can be obtained from the known mass and frequency ratios. In this way values in the range $4.5-4.9\times10^{-3}$ Å^2 are found. Thus the correct values for the Pd σ^2 are likely to be smaller than previously reported. It is very important that an EXAFS data-analysis based on theoretical signals is able to fit absolute variance parameters.

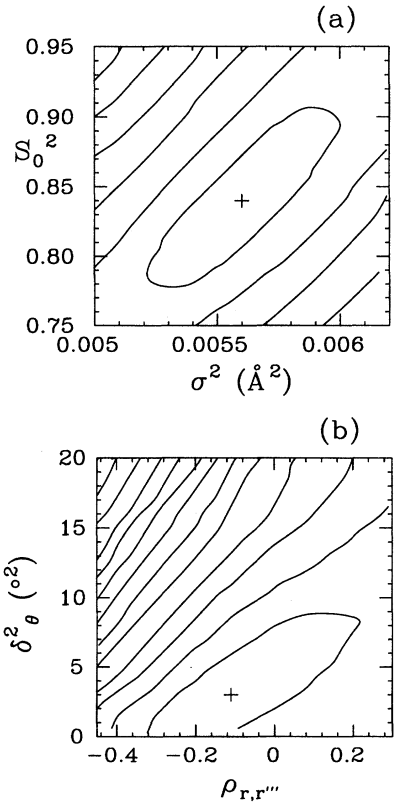

FIG. 10. Correlation maps for the best fit of the Pd foil spectrum at 296 K, (a) contour map between σ^2 and S_0^2, (b) contour map between $\rho_{r,r'''}$ and $\delta^2_{1\theta}$. The inner elliptical curves correspond to the intersection of the 95% p-dimensional confidence interval with the corresponding two-parameter plane.

The error analysis for the three-body parameters indicates in general relatively large statistical errors, this is due to the relative weakness of the signal, in this case. In particular it is not possible to determine exactly the parameters for the 120° triangle. Instead, as expected, the parameters for the 180° triangle can be more accurately determined. The correlation map between δ^2_θ and $\rho_{r,r'''}$ is shown in Fig. 10(b). The 95% confidence interval indicates clearly that the vibration of the configuration departs only slightly from collinearity $\delta^2_\theta \leqslant 10^{\circ 2}$ with a tendency to a negative correlation between adjacent bond vibrations $\rho_{r,r'''}=-0.1(3)$. A similar situation was observed in the collinear configuration present in the bcc Fe.[31] The slightly negative value is expected and reflects the fact that the fourth-shell variance is slightly smaller than twice the first-shell variance. Again, another example has been reported where it is possible to extract triplet correlation information in the correct framework of the statistical error analysis.

VII. CONCLUSION

In the present paper the fitting methodology adopted within the GNXAS approach for multiple-scattering EXAFS data analysis is described in details. Several prototypical examples of applications of GNXAS have been presented. All this material complements the theoretical aspects discussed in the previous paper.[14] The major scientific advances achieved by the present investigations can be summarized by the following four points.

(1) The procedure to estimate random errors in the fitting parameters and to perform a complete evaluation of the results based on the application of statistical test has been described and illustrated with several examples.

(2) A powerful fitting approach that allows us to include in a systematic way n-body MS contributions in the modeling of the EXAFS spectra has been presented. Equilibrium and vibrational three-body parameters connected with precise physical quantities are introduced in typical molecular or crystalline cases. Specific examples including several three-body terms demonstrate that the number of fitting parameters does not increase in an uncontrolled manner.

(3) Error analysis indicates that the typical accuracy reachable in the case of simple molecules for distances and vibrational amplitudes is comparable with that of electron diffraction and that there are no systematic errors due to approximations in the theory at this level of sensitivity. Similarly bond distances in test crystalline cases are found to be in agreement with known crystallographic structures. At this level of accuracy (in the 0.001 Å range) experimental systematic errors due to the approximate monochromator cali-

bration and scan inaccuracy can be detectable. It is therefore recommended to use advanced monochromator setups that allow one to perform an the absolute energy calibration of the beam like the one presented by Pettifer and Hermes.[65]

(4) Finally, the possibility to fit geometrical and vibrational parameters associated with three-body configurations has been unambiguously demonstrated taking advantage of the extensive application of statistical tests to EXAFS data analysis. This represents a fundamental step towards the exploitation of the XAS sensitivity to higher-order distributions in condensed matter.

All these results are a main contribution to the advances in the XAS technique and data-analysis procedures. In light of the success of the GNXAS methodology and its intrinsic potential we believe that the adoption of the suggested procedures will certainly be useful in several applied problems. Consequently we propose to adopt them as a standard for EXAFS data analysis.

---

*Present address: E.S.R.F., BP 220, F-38043 Grenoble Cedex, France.

[1] P. A. Lee, P. Citrin, P. Eisenberger, and B. Kincaid, Rev. Mod. Phys. **53**, 769 (1981); B. K. Teo and D. C. Joy, *EXAFS Spectroscopy, Techniques and Applications* (Plenum, New York, 1981); T. M. Hayes and J. B. Boyce, in *Solid State Physics*, edited by H. Eherenreich, F. Seitz, and D. Turnbull (Academic, New York, 1982), Vol. 37, p. 173; D. C. Koningsberger and R. Prins, *X-ray Absorption* (Wiley, New York, 1988).

[2] F. W. Lytle, D. E. Sayers, and E. A. Stern, Physica B **158**, 701 (1989); *X-Ray Absorption Fine Structure*, edited by S. S. Hasnain (Ellis Horwood, York, 1991), pp. 751–770.

[3] S.-H. Chou, J. J. Rehr, E. A. Stern, and E. R. Davidson, Phys. Rev. B **35**, 2604 (1987); Dan Lu and J. J. Rehr, *ibid.* **37**, 6126 (1988).

[4] T. A. Tyson, K. O. Hodgson, C. R. Natoli, and M. Benfatto, Phys. Rev. B **46**, 5997 (1992).

[5] S. J. Gurman, N. Binsted, and I. Ross, J. Phys. C **19**, 1845 (1986).

[6] M. Benfatto, C. R. Natoli, A. Bianconi, J. Garcia, A. Marcelli, M. Fanfoni, and I. Davoli, Phys. Rev. B **34**, 5774 (1986).

[7] C. R. Natoli and M. Benfatto, J. Phys. (Paris) Colloq. **47**, C8-11 (1986).

[8] J. J. Rehr, R. C. Albers, and S. I. Zabinsky, Phys. Rev. Lett. **69**, 3397 (1992).

[9] J. J. Rehr and C. R. Albers, Phys. Rev. B **41**, 8139 (1990).

[10] A. Filipponi, J. Phys. Condens. Matter **3**, 6489 (1991).

[11] N. Binsted, J. W. Campbell, S. J. Gurman, and P. C. Stephenson, The Daresbury Laboratory EXCURVE program, Daresbury Laboratory, Warrington WA4 4AD, England.

[12] The acronym GNXAS derives from g_n (the n-body distribution functions) and XAS (x-ray-absorption spectroscopy).

[13] A. Filipponi, A. Di Cicco, T. A. Tyson, and C. R. Natoli, Solid State Commun. **78**, 265 (1991).

[14] A. Filipponi, A. Di Cicco, and C. R. Natoli, preceding paper, Phys. Rev. B **52**, 15 122 (1995).

[15] A. I. Frenkel, E. A. Stern, M. Qian, and M. Newville, Phys. Rev. B **48**, 12 449 (1993).

[16] A. I. Frenkel, E. A. Stern, A. Voronel, M. Qian, and M. Newville, Phys. Rev. Lett. **71**, 3485 (1993).

[17] J. Mustre de Leon, J. J. Rehr, S. I. Zabinsky, and R. C. Albers, Phys. Rev. B **44**, 4146 (1991); J. J. Rehr, J. Mustre de Leon, S. I. Zabinsky, and R. C. Albers, J. Am. Chem. Soc. **113**, 5135 (1991).

[18] A. Di Cicco, S. Stizza, A. Filipponi, F. Boscherini, and S. Mobilio, J. Phys. B **25**, 2309 (1992).

[19] P. D' Angelo, A. Di Cicco, A. Filipponi, and N. V. Pavel, Phys. Rev. A **47**, 2055 (1993).

[20] E. Burattini, P. D' Angelo, A. Di Cicco, A. Filipponi, and N. V. Pavel, J. Phys. Chem. **97**, 5486 (1993).

[21] A. Filipponi, L. Lozzi, M. Passacantando, P. Picozzi, and S. Santucci, Phys. Rev. B **47**, 8494 (1993).

[22] A. Di Cicco and M. Berrettoni, Phys. Lett. A **176**, 375 (1993).

[23] A. Filipponi, A. Di Cicco, M. Benfatto, and C. R. Natoli, J. Non-Cryst. Solids **114**, 229 (1989); Europhys. Lett. **13**, 319 (1990).

[24] L. Ottaviano, A. Filipponi, A. Di Cicco, S. Santucci, and P. Picozzi, J. Non-Cryst. Solids **156-158**, 112 (1993).

[25] A. Di Cicco and A. Filipponi J. Non-Cryst. Solids **156-158**, 102 (1993).

[26] A. Di Cicco and A. Filipponi, Europhys. Lett. **27**, 407 (1994).

[27] A. Filipponi and A. Di Cicco, Phys. Rev. B **51**, 12 322 (1995).

[28] A. Filipponi, L. Ottaviano, M. Passacantando, P. Picozzi, and S. Santucci, Phys. Rev. E **48**, 4575 (1993).

[29] P. D' Angelo, A. Di Nola, A. Filipponi, N. V. Pavel, and D. Roccatano, J. Chem. Phys. **100**, 985 (1994).

[30] A. Filipponi, P. D' Angelo, N. V. Pavel, and A. Di Cicco, Chem. Phys. Lett. **225**, 150 (1994).

[31] A. Di Cicco, M. Berrettoni, S. Stizza, E. Bonetti, and G. Cocco, Phys. Rev. B **50**, 12 386 (1994).

[32] A. Filipponi, A. Di Cicco, R. Zanoni, M. Bellatreccia, V. Sessa, C. Dossi, and R. Psaro, Chem. Phys. Lett. **184**, 485 (1991).

[33] E. Nordlander, Sonny C. Lee, Wei Cen, Z. Y. Wu, C. R. Natoli, A. Di Cicco, A. Filipponi, B. Hedman, K. O. Hodgson, and R. J. Holm, J. Am. Chem. Soc. **115**, 5549 (1993); S. D. Conradson, B. K. Burgess, W. E. Newton, A. Di Cicco, A. Filipponi, J. Wu, C. R. Natoli, B. Hedman, and K. O. Hodgson, Proc. Nat. Acad. Sci. USA **91**, 1290 (1994); H. I. Liu, A. Filipponi, N. Gavini, B. K. Burgess, B. Hedman, A. Di Cicco, C. R. Natoli, and K. O. Hodgson, J. Am. Chem. Soc. **116**, 2418 (1994); T. E. Westre, A. Di Cicco, A. Filipponi, C. R. Natoli, B. Hedman, E. I. Solomon, and K. O. Hodgson, *ibid.* **116**, 6757 (1994).

[34] J. J. Rehr, E. A. Stern, R. L. Martin, and E. R. Davidson, Phys. Rev. B **17**, 560 (1978).

[35] A. Filipponi, E. Bernieri, and S. Mobilio, Phys. Rev. B **38**, 3298 (1988).

[36] S. Bodeur, P. Millié, E. Lizon à Lugrin, I. Nenner, A. Filipponi, F. Boscherini, and S. Mobilio, Phys. Rev. A **39**, 5075 (1989).

[37] A. Filipponi, T. A. Tyson, K. O. Hodgson, and S. Mobilio, Phys. Rev. A **48**, 1328 (1993).

[38] A. Filipponi, L. Ottaviano, and T. A. Tyson, Phys. Rev. A **48**, 2098 (1993); A. Di Cicco and A. Filipponi, Phys. Rev. B **49**, 12 564 (1994).

[39] A. Filipponi and A. Di Cicco, Phys. Rev. A **52**, 1072 (1995).

[40] S. J. Schaphorst, A. F. Kodre, J. Ruscheinski, B. Crasemann, T. Åberg, J. Tulkki, M. H. Chen, Y. Azuma, and G. S. Brown, Phys. Rev. A **47**, 1953 (1993).

[41] A. Filipponi, S. Di Nardo, M. Passacantando, L. Lozzi, S. Santucci, and P. Picozzi, Phys. Rev. B **48**, 13 430 (1993); A. Di Cicco, M. De Crescenzi, R. Bernardini, and G. Mancini, Phys. Rev. **49**, 2226 (1994); A. Filipponi, M. Passacantando, L. Lozzi,

S. Santucci, P. Picozzi, and A. Di Cicco, Solid State Commun. **91**, 555 (1994).
[42] A. Filipponi, Physica B **208&209**, 29 (1995).
[43] B. Beagley, in *Stereochemical Applications of Gas-phase Electron Diffraction*, edited by I. Hargittai and M. Hargittai (VCH, New York, 1988), p. 436.
[44] G. Li, F. Bridges, and G. S. Brown, Phys. Rev. Lett. **68**, 1609 (1992).
[45] M. Newville, P. Līviņš, Y. Yacoby, J. J. Rehr, and E. A. Stern, Phys. Rev. B **47**, 14 126 (1993).
[46] A. Filipponi, J. Phys. Condens. Matter **6**, 8415 (1994).
[47] R. W. Joyner, K. J. Martin, and P. Meehan, J. Phys. C **20**, 4005 (1987).
[48] E. A. Stern, Phys. Rev. B **48**, 9825 (1993).
[49] M. Lampton, B. Margon, and S. Bowyer, Astrophys. J. **208**, 177 (1976); Y. Avni, *ibid.* J. **210**, 642 (1976).
[50] CERN Program Library Long Writeup D506, MINUIT reference manual, Geneva, 1992.
[51] A. Filipponi, J. Phys. Condens. Matter (to be published).
[52] W. C. Hamilton, Acta Crystallogr. **18**, 502 (1965).
[53] A. J. Dent, P. C. Stephenson, and G. N. Greaves, Rev. Sci. Instrum. **63**, 856 (1992); G. N. Greaves, A. J. Dent, B. R. Dobson, S. Kalbitzer, S. Pizzini, and G. Müller, Phys. Rev. B **45**, 6517 (1992).
[54] B. M. Kincaid and P. Eisenberger, Phys. Rev. Lett. **34**, 1361 (1975); S. M. Heald and E. A. Stern, Phys. Rev. B **17**, 4069 (1978); E. A. Stern, S. M. Heald, and B. Bunker, Phys. Rev. Lett. **42**, 1372 (1979).
[55] A. Di Cicco, M. Berrettoni, R. Marassi, R. Tossici, and A. Filipponi, in *Proceedings of the Ninth International Symposium on Molten Salts*, edited by C. L. Hussey, D. S. Newman, G. Mamantov, and Y. Ito (Electrochemical Society, New York, 1994), Vol. 94–13, p. 77.
[56] K. Kuchitsu, Bull. Chem. Soc. Jpn. **40**, 498 (1967).
[57] A. I. Frenkel, E. A. Stern, A. Voronel, M. Qian, and M. Newville, Phys. Rev. B **49**, 11 662 (1994).
[58] Y. Morino and T. Iijima, Bull Chem. Soc. Jpn. **35**, 1661 (1962).
[59] A. Bianconi, A. Di Cicco, N. V. Pavel, M. Benfatto, A. Marcelli, C. R. Natoli, P. Pianetta, and J. Woicik, Phys. Rev. B **36**, 6426 (1987).
[60] J. A. McCaulley, Phys. Rev. B **47**, 4873 (1993).
[61] T. Yokoyama, S. Kimoto, and T. Ohta, Jpn. J. Appl. Phys. **28**, L851 (1989).
[62] E. Sevillano, H. Meuth, and J. J. Rehr, Phys. Rev. B **20**, 4908 (1979).
[63] E. C. Svensson, B. N. Brockhouse, and J. M. Rowe, Phys. Rev. **155**, 619 (1967).
[64] A. P. Miiller and B. N. Brockhouse, Can. J. Phys. **49**, 704 (1971).
[65] R. F. Pettifer and C. Hermes, J. Appl. Crystallogr. **18**, 404 (1985); J. Phys. (Paris) Colloq. **47**, C8-127 (1986).